Fiber-coupled, Littrow-grating cavity displacement sensor

Graham Allen,* Ke-Xun Sun, and Robert Byer

Hansen Experimental Physics Laboratory, Stanford University, Stanford, California 94305-4085, USA
**Corresponding author: gsallen@stanfordalumni.org*

Received January 11, 2010; accepted February 9, 2010;
posted March 8, 2010 (Doc. ID 122498); published April 15, 2010

We have demonstrated a compact, optical-fiber-fed, optical displacement sensor utilizing a Littrow-mounted diffraction grating to form a low-finesse Fabry–Perot cavity. Length changes of the cavity are read out via the Pound–Drever–Hall rf modulation technique at 925 MHz. The sensor has a nominal working distance of 2 cm and a total dynamic range of 160 nm. The displacement noise floor was less than 3×10^{-10} m/$\sqrt{\text{Hz}}$ above 10^{-2} Hz, limited by the frequency drift of the reference laser. A frequency-stabilized laser would reduce the noise floor to below 10^{-12} m/$\sqrt{\text{Hz}}$. The use of a 925 MHz modulation frequency demonstrates high-precision readout of a low-finesse compact resonant cavity. © 2010 Optical Society of America

OCIS codes: 060.2370, 050.2230, 280.4788.

Interferometric displacement sensors with subnanometer resolution have been developed for a wide variety of applications, such as gravitational-wave detection [1–3] and atomic force microscopy [4,5]. Free-space displacement sensors using optical fiber have demonstrated subnanometer resolution, but these sensors utilized a working distance less than 5 μm [4–6].

We use a low-finesse, free-space Fabry–Perot cavity formed by a Littrow mounted diffraction grating and an optical flat attached to the reference object and add the use of the Pound–Drever–Hall (PDH) rf readout technique to achieve high precision with a 2 cm working distance [7]. The sensor has a dynamic range of 160 nm and a noise floor less than 2×10^{-12} m/$\sqrt{\text{Hz}}$ above 2 Hz.

The sensor presented here has several innovations that make it unique as a displacement sensor. The reference surface is a diffraction grating mounted at the Littrow angle. This changes the geometry of the Fabry–Perot cavity, since the diffractive grating simultaneously acts as a folding mirror and the input optic for the cavity. This allows for a more compact physical layout and allows measurements from both sides of the grating [8]. The sensor uses an optical fiber for delivery and recovery of the displacement signal, eliminating the need for active optical components in the sensor head. This allows the laser, modulator, and detector to all be located remotely and eliminates the need for active elements in the sensor head. The 925 MHz modulation frequency is the highest reported PDH modulation frequency, to our knowledge.

The use of a diffraction grating to form an all-reflective optical interferometer was demonstrated in 1998 by Sun and Byer [2]. Recent developments in high-efficiency diffractive gratings have focused on high-finesse Fabry–Perot cavities [9,10]. When used as a displacement sensor, the high-finesse cavity is extremely sensitive but has a very small dynamic range of a few nanometers. To achieve a maximum range exceeding 100 nm, we use a diffraction grating in a low-finesse configuration [11]. In this Letter, we describe our progress in refining the sensor with the addition of rf readout. Rf phase readout offers lower noise and provides true null operation, which is essential for high-precision operation.

The core of the sensor is a diffractive Fabry–Perot cavity that is reflectively sensed using the PDH rf modulation technique [7,12]. A fiber-optic phase modulator is used to apply rf sidebands to the main beam, and the measured signal is the phase shift of the center frequency with respect to its sidebands. The phase information is encoded in a signal at the carrier-sideband beat frequency, so a high-speed photodetector is required to detect the rf beat note. The rf signal is then mixed with the rf drive to convert the signal to baseband for digitization.

In a high-finesse cavity, the sideband frequency exceeds the cavity bandwidth and the sidebands are assumed to be totally reflected by the cavity. In the low-finesse cavity demonstrated here, the 925 MHz sidebands are still well within the cavity resonance. Our modulation frequency is limited to less than 1 GHz by the bandwidth of our photodetector, as a result we operated with a modulation frequency of 925 MHz. Although the sidebands are still partially resonant, there is excellent phase separation between the reflected sidebands and the carrier. Higher modulation frequencies would improve the phase separation and increase the reflected sideband power, potentially increasing the PDH signal by up to a factor of 2. High-speed photodetectors could allow modulation at frequencies in excess of 5 GHz, allowing for PDH locking to small, low-finesse cavities. The sensor operates in an open-loop configuration where the PDH signal is a direct measurement of the cavity length. The PDH signal provides a position readout that is approximately linear across the cavity resonance.

Figure 1 shows a diagram of the experimental implementation of the Littrow grating cavity sensor. The Fabry–Perot cavity is formed between a high-efficiency 900 lines/mm diffraction grating (Newport 05HG900-800-1) and a 12.8 mm mirror mounted on a piezoelectric transducer (PZT) as a reference surface. The cavity length is 1.75 cm, corresponding to a free-spectral range of 8.5 GHz. The gradient-index

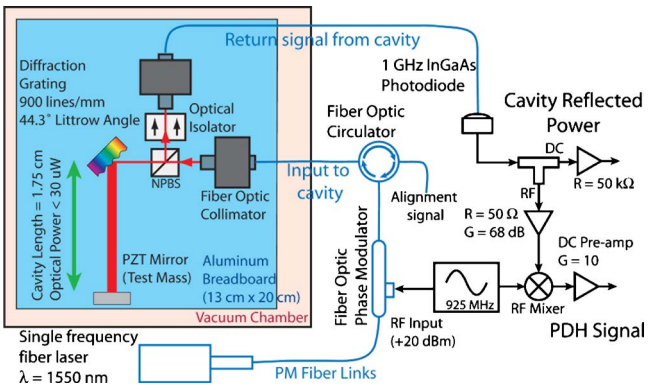

Fig. 1. (Color online) Diagram of the experiment setup. The GRIN lens and cavity are separated from the other components by approximately 1 m of polarization maintaining fiber optic cable.

(GRIN) lens is aligned so that the input light is polarized for minimum diffraction efficiency of the grating, giving the cavity a finesse of roughly $\mathcal{F}=3$. All of the bulk optical components are mounted on a 13 cm $\times$ 20 cm aluminum breadboard, which is then placed into a 0.1 Torr vacuum chamber to minimize disturbances due to air currents and thermal drift. The use of a fiber-optic GRIN lens for input and output coupling allows for a compact sensor-head inside the vacuum chamber and eliminates alignment drifts arising from coupling through vacuum windows. Compact optical mounts could significantly shrink the sensor head, allowing it to fit into a $4\times4\times3$ cm^3 volume.

A 1550 nm single-frequency fiber laser (NP Photonics Scorpion) with a free-running linewidth of approximately 5 kHz provides the input light. An adjustable air-gap attenuator reduces the 30 mW of laser power down to 10–200 μW for the sensor. A 10 GHz fiber optic phase modulator applies the 925 MHz rf sidebands. The light is delivered to the cavity via a fiber optic circulator and a GRIN lens collimator. The reflected light from the cavity is recollimated by a return GRIN lens and delivered to a fiber-coupled InGaAs photodiode (Thorlabs D400FC). The free-space beamsplitter reduces the reflected signal by 50%, which combined with the collimating efficiency of the GRIN lens, results in 35% of the reflected light reaching the photodetector.

The reflected signal from the circulator is used for initial alignment and can be used as a secondary monitor. Residual feedthrough from ports $1\rightarrow3$ in the circulator caused coherent reflections for the signal at port 3 and a significant increase in noise. The free-space beams plitter diverts the reflected signal directly at the sensor head, isolating the return signal from interference with the input beam. An optical isolator is placed directly before the return fiber input to suppress any interference between reflections in the return fiber and the cavity. Angle-polished connectors or fusion splices are used throughout the system to minimize reflections and spurious interferometers. Approximately 2 m of optical fiber is used for the inbound and reflected optical signals.

The beat signal between the carrier and sidebands is detected by a broadband photodetector with 1 GHz bandwidth. The dc photocurrent signal is separated at the photodetector and used as a diagnostic. The photodetector has a 50 Ω transimpedance gain, requiring 68 dB of rf amplification to match the mixer input level. The beat signal is mixed against the phase-modulator rf drive signal. The phase between the reference oscillator and the photodetector beat note is adjusted by tuning the oscillator frequency, taking advantage of the differential rf path length between the inputs to the mixer. A dc bias-T is used to separate the PDH signal after it has been mixed down to baseband. The dc PDH signal is then amplified and low-pass filtered by a dc preamplifier prior to digitization.

Figure 2 shows a scan of the mirror across the cavity resonance. The region of the PDH signal used for displacement sensing is indicated by the solid red line. The PDH response is linearized by assuming a linear PZT scan. Once the scan is captured, the piezo is disabled and the cavity is allowed to freely drift.

The root-mean power-spectral density of the Littrow cavity sensor's drift is shown in Fig. 3. Above 1 Hz, the fundamental noise floor of the sensor is the photodetector, as shown in the 150 Hz to 300 Hz band. This demonstrates the fundamental sensor resolution is better than 1 pm/$\sqrt{\text{Hz}}$. The excess noise spikes below 150 Hz and above 300 Hz are a result of acoustic vibrations of the measurement platform and not an indication of the sensor noise floor, because these disturbances cause physical-cavity length changes.

For use as an displacement sensor at very low frequency (below 1 Hz) there are several sources of drift that introduce excess noise. Figure 4 shows the root-mean power-spectral density of noise at frequencies below 10 Hz. The rolloff at the 3 Hz low-pass filter is set to prevent aliasing of 60 Hz line noise, which is disabled for the measurements shown in Fig. 3.

Below 1 Hz, the sensor noise floor is limited by the frequency drift of the laser used as a length reference. Displacement noise due to laser frequency drift is estimated using a combination of manufacturer's data on the laser frequency stability and direct measurement of the coupling between laser frequency noise and displacement for the Littrow sensor. The

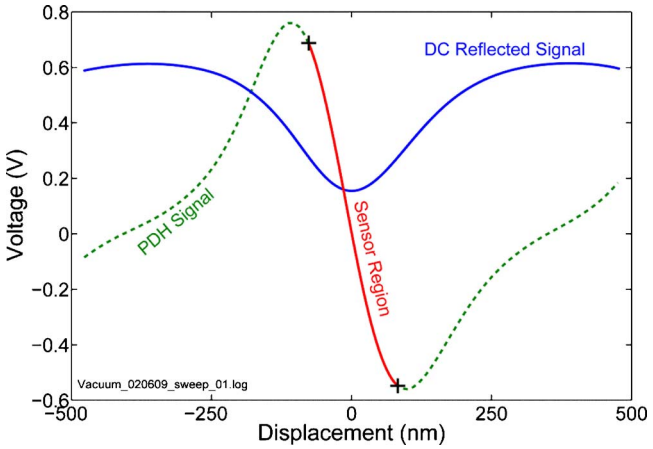

Fig. 2. (Color online) Experimental calibration curve for the Littrow grating cavity sensor.

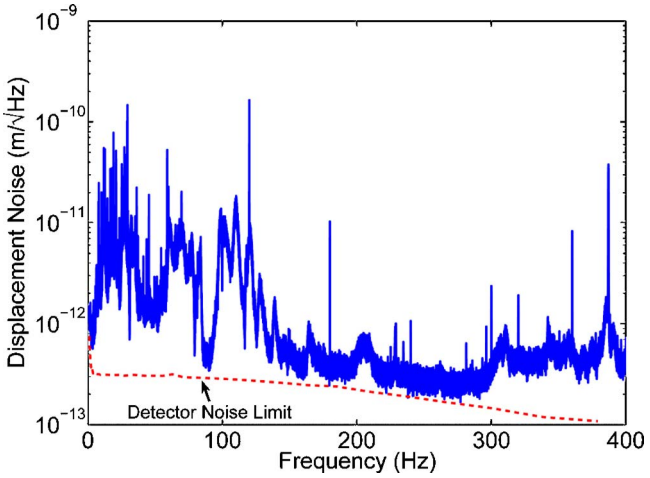

Fig. 3. (Color online) Measured noise spectrum of the Littrow grating cavity sensor from 1 Hz to 400 Hz. From 150 Hz to 300 Hz, the sensor noise floor is less than 1 pm/$\sqrt{\text{Hz}}$ as determined by the detector noise floor.

Fabry–Perot cavity eliminates the need for a stable reference arm but places more-stringent restrictions on the wavelength stability of the laser source, especially when used with cavity lengths in excess of 1 mm.

At the lowest frequencies, below 10^{-3} Hz, the sensor performance is limited by the thermal stability of the optical mounts forming the cavity. The optical platform has a thermal time constant of 120 min, leading to a sharp rolloff in the thermal drift for frequencies above 10^{-4} Hz. The thermal drift leads to a sharp increase in the noise floor at frequencies below 10^{-3} Hz.

For measurements at very low frequency, the most important improvements are a frequency-stabilized laser to serve as a length reference, and eliminating $1/f$ drifts in electronics. For measurements above 1 kHz, the Johnson noise of the photodetector is currently limiting the performance of the sensor well above the quantum-mechanical optical shot noise limit. Replacing the photodiode with an avalanche photodiode (APD) would increase the photocurrent by approximately a factor of 10, equivalently reducing the detector noise by a factor of 10. High-speed APDs with bandwidths exceeding 1 GHz have been developed for the telecommunications industry and would be an ideal detector. A resonant rf-tuned photodetector circuit could have a transimpedance gain of 500 Ω, substantially improving the signal-to-noise ratio.

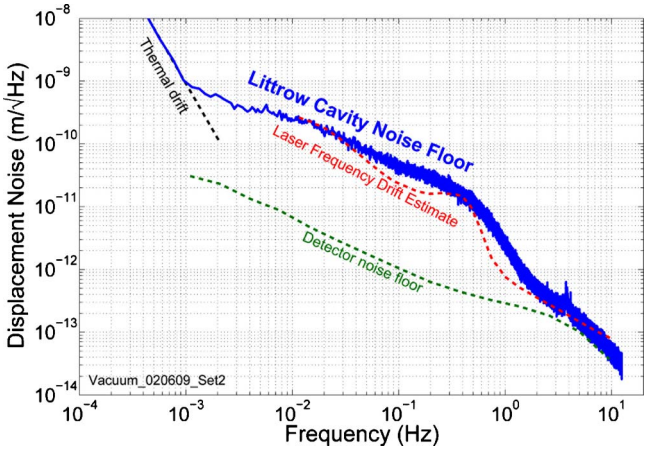

Fig. 4. (Color online) Measured noise spectrum of the Littrow grating cavity sensor. The performance of the sensor is limited by the frequency stability of the laser used a length reference and by the detector noise above 1 Hz.

The Littrow grating cavity sensor performance exceeds 3 pm/$\sqrt{\text{Hz}}$ above 1 Hz. Below this frequency, the performance of the sensor is limited by the frequency stability of the reference laser. A laser with frequency stability greater than 15 kHz/$\sqrt{\text{Hz}}$ would allow for performance better than 3 pm/$\sqrt{\text{Hz}}$. This level of frequency stability can be achieved with the use of a high-finesse reference cavity or by locking to a molecular gas transition such as methane or CO [13,14].

The low-cavity finesse does allow for a wide dynamic range, exceeding ±70 nm but does not offer significantly increased sensitivity when compared with Michelson-type interferometric sensors. The use of a resonant cavity instead eliminates the need for a stable reference arm, ensuring that the displacement measurement is a direct measurement relative to a known reference surface.

We have demonstrated PDH readout of a a fiber-coupled, diffractive resonant cavity with a linewidth greater than 2 GHz using a modulation frequency of 925 MHz. To our knowledge, this is the largest reported cavity linewidth used with the PDH technique and demonstrates that the PDH technique can be applied to compact cavities that were previously interrogated only via fringe sidelocking.

References

1. M. B. Gray, D. E. McClelland, M. Barton, and S. Kawamura, Opt. Quantum Electron. **31**, 571 (1999).
2. K.-X. Sun and R. L. Byer, Opt. Lett. **23**, 567 (1998).
3. C. C. Speake and S. M. Aston, Class. Quantum Grav. **22**, S269 (2005).
4. D. Rugar, H. J. Mamin, and P. Guethner, Appl. Phys. Lett. **55**, 2588 (1989).
5. S. Breen, B. E. Paton, B. L. Blackford, and M. H. Jericho, Appl. Opt. **29**, 16 (1990).
6. T. Wang, S. Zheng, and Z. Yang, Sens. Actuators, A **69**, 134 (1998).
7. R. W. P. Drever, J. L. Hall, F. V. Kowalski, J. Hough, G. M. Ford, A. J. Munley, and H. Ward, Appl. Phys. B **31**, 97 (1983).
8. K.-X. Sun, G. Allen, S. Buchman, D. DeBra, and R. Byer, Class. Quantum Grav. **22**, S287 (2005).
9. D. Friedrich, O. Burmeister, A. Bunkowski, T. Clausnitzer, S. Fahr, E.-B. Kley, A. Tünnermann, K. Danzmann, and R. Schnabel, Opt. Lett. **33**, 101 (2008).
10. P. P. Lu, K.-X. Sun, R. L. Byer, J. A. Britten, H. T. Nguyen, J. D. Nissen, C. C. Larson, M. D. Aasen, T. C. Carlson, and C. R. Hoaglan, Opt. Lett. **34**, 1708 (2009).
11. G. Allen, K.-X. Sun, and R. Byer, AIP Conf. Proc. **873**, 334 (2006).
12. E. D. Black, Am. J. Phys. **69**, 79 (2001).
13. P. Balling, M. Fischer, P. Kubina, and R. Holzwarth, Opt. Express **13**, 9196 (2005).
14. W. C. Swann and S. L. Gilbert, J. Opt. Soc. Am. B **19**, 2461 (2002).